Cirrus Microphysical Properties and Air Motion Statistics Using Cloud Radar Doppler Moments. Part II: Climatology

MIN DENG

University of Wyoming, Laramie, Wyoming

GERALD G. MACE

University of Utah, Salt Lake City, Utah

(Manuscript received 16 January 2008, in final form 15 May 2008)

ABSTRACT

The algorithm described in Part I has been applied to the millimeter cloud radar observations from January 1999 to December 2005 at the Atmospheric Radiation Measurement Program (ARM) Southern Great Plains (SGP) and Tropical Western Pacific (including Manus and Nauru) sites. Approximately 10 000 cirrus hours from each of these sites were analyzed. Retrieved cloud properties including condensed mass, particle size, optical depth, and in-cloud vertical air motions were analyzed in terms of their geographical, seasonal, and diurnal variations. The analysis shows that tropical ice clouds observed by millimeter radar are very different from ice clouds at SGP, with the tropical clouds having slightly larger particle sizes and greater ice masses and being more likely to be associated with ascending air motions, in addition to being colder and higher in altitude. A positive residual of derived in-cloud air motion found in the tropical data likely provides evidence for lofting of air into the tropopause transition layer as a result of radiative heating. The midlatitude cirrus demonstrate strong seasonal variations with more frequent, thicker clouds occurring during the summer than during the winter. Very subtle seasonal variations are found for tropical ice clouds, and evidence is presented that cirrus properties vary interannually and are correlated with El Niño oscillations. In addition, it is found that tropical cirrus demonstrate a stronger diurnal cycle than cirrus of the midlatitudes, with the in-cloud updrafts peaking in the early afternoon.

1. Introduction

Ice clouds of the upper troposphere, hereinafter referred to as cirrus, are known to play a key role in the radiative balance of Earth (Stephens et al. 1990; Ackerman et al.1988) because the infrared greenhouse and solar albedo effects depend on both microphysical (condensed water mass and effective particle size) and macroscopic properties (cloud cover and vertical location). These properties are poorly represented in numerical models, and many outstanding issues regarding cirrus occurrence and evolution remain to be understood to the degree that they can be parameterized in numerical models. The main uncertainties stem from the complexities in relating cirrus properties to atmospheric motions. Del Genio (2002) cites the following issues: 1) cirrus encompass a wide range of optical thicknesses and altitudes, 2) the underlying dynamical processes that create cirrus are poorly understood and differ in different parts of the earth, 3) prediction of cirrus formation depends on accurate predictions of water vapor mixing ratios and the concentration of nucleating particles, and 4) cirrus are more difficult to observe than other cloud types, making the outstanding issues more difficult to address. Recent investigations show that understanding the subgrid-scale cloud physics may be even more critical than increasing the model resolution (Duffy et al. 2006). Therefore, it is necessary to continue to study cirrus cloud properties as well as the associated cloud dynamical processes.

According to Sassen (2002), a breakdown of natural cirrus cloud–generating mechanisms includes 1) a variety of synoptic-scale disturbances (jet stream, closed upper-level lows, frontal overriding, etc.) that have in common relatively weak average vertical lifting rates

Corresponding author address: Min Deng, Department of Atmospheric Science, University of Wyoming, 1000 E. University Ave., Laramie, WY 82071.
E-mail: mdeng2@uwyo.edu

DOI: 10.1175/2008JAMC1949.1

© 2008 American Meteorological Society

and generally involve top-down growth; 2) injection, or anvil cirrus from strong thunderstorm updrafts; 3) orographic wave cloud cirrus induced by local terrain, also with potentially strong vertical motion; and 4) tropopause transition layer (TTL; Gettleman et al. 2002) cirrus that seem to inhabit vast geographical regions near the cold tropical tropopause. TTL cirrus are often very tenuous and are generally not detected by millimeter radar (Comstock et al. 2002) and are therefore not considered in this paper. The tropical cirrus clouds studied here include clouds that occur predominantly in the 10–15-km layer, that is, the layer in which the majority of the deep tropical convective towers detrain (Sherwood and Dessler 2003). These clouds differ in several substantial ways from TTL cirrus in that they tend to contain more condensed mass, are optically thicker, and demonstrate much greater variability horizontally, vertically, and temporally. They also tend to be more directly attributable to outflows from deep convection at some point in the past (Mace et al. 2006b).

These distinctions in cloud microphysical, macrophysical, and radiative properties are essentially functions of ambient temperature, the strength of updraft and/or lifting velocities, and the source of the condensate and cloud-forming nuclei. These properties in turn depend on the meteorological processes that generate cirrus and, therefore, depend fundamentally on geographic locations. The seasonal dependence of cirrus frequency and characteristics is clearly a reflection of the basic synoptic patterns that control the large-scale meteorological behavior (Mace et al. 2006a). For instance, as Mace et al. (2006b) and Massie et al. (2002) found, about 50% of tropical ice clouds have been associated with deep convection at some point in their history whereas the origin of the other 50% is unknown. In the midlatitudes, the properties of the cirrus appear to be more a function of the large-scale vertical motion history along the trajectories followed by the cloud system (Mace et al. 2006a).

In Deng and Mace (2006, hereinafter referred to as Part I), we describe an algorithm that uses the moments of the Doppler spectrum to derive both the microphysical properties of cirrus and the ambient air motion of the cloud volume. This approach assumes that the cirrus particle size distribution can be described as a single-mode gamma function of some specified order and that the spectrum of turbulent air motion can be described as a double-sided exponential function centered on some ambient up- or downdraft. In this article (Part II), we evaluate cirrus cloud properties derived from this algorithm in the midlatitudes and tropics (section 2). The cloud properties and derived cloud-scale air motions are analyzed in terms of seasonal and diurnal variations and then are compared between the midlatitudes and tropics.

2. Data overview

To provide a better understanding of cloud processes and their radiative effects on Earth's climate system so that these processes can be more faithfully represented in climate models, the U.S. Department of Energy's Atmospheric Radiation Measurement (ARM) Program (Ackerman and Stokes 2003) has conducted long-term surface observations using a suite of passive and active remote sensors at the ARM Climate Research Facilities (ACRF). In this study we use data collected at the Southern Great Plains (SGP) and Tropical Western Pacific (TWP) sites. The SGP ACRF was chosen as the first ARM field measurement site in 1992 because of its relatively homogenous geography and strong seasonality. The TWP sites include Manus (TWPC1; 1.06°S, 147.4°E) and Nauru (TWPC2; 0.52°S, 166.92°E). Considering the large-scale environment of these equatorial longitudes, Manus lies within the tropical western Pacific Ocean warm pool. Nauru is located at the eastern edge of the warm pool in a region of generally suppressed convective activity. However, Nauru may be more sensitive to tropical interseasonal variations such as the El Niño–Southern Oscillation (ENSO). The long-term observations at these sites provide a unique opportunity to study the geographical, interannual, and shorter-time-scale dependence of cirrus cloud properties and processes.

a. The MMCR measurements and retrieval algorithm

The millimeter-wave cloud radar (MMCR) at the SGP site has been described by Moran et al. (1998) and Clothiaux et al. (1995). The radar operates at a frequency of 34.86 GHz (Ka band) with a stated calibration uncertainty of less than approximately 1–2 dB in reflectivity and 10 cm s^{-1} in mean Doppler velocity and spectrum width. The antenna diameter is 3 m with 57.48-dB gain at the SGP site where the minimum detectable signal is approximately −50 dBZe at 5-km range. The MMCRs at the TWP sites are similar except that their antenna diameters are 2 m with 52.73-dB gain, which makes the MMCR at the SGP site more sensitive by approximately 5 dB. The MMCR used in this study are vertically pointing to within 0.01° of zenith (K. B. Widener 2008, personal communication) so that the Doppler moments contain information regard-

ing the fall speed of the ice crystals and the vertical air motion.

Cirrus cloud identification at SGP is based on the definition of cirrus in Mace et al. (2001). Cirrus identification at the TWP sites is adapted from these criteria. We require the radar echo top to occur at a temperature colder than −35°C, the layer base must be higher than 7 km (which is approximately 400 hPa and a temperature of −10°C), the maximum dBZe in the layer must occur at a temperature colder than −22°C, and the cloud-layer depth must be larger than 180 m or two range bins. As described in Mace et al. (2001), this definition, although arbitrary, helps to exclude deep cloud layers that are not normally classified as cirrus.

The algorithm to retrieve the cirrus microphysical properties and vertical motion as well as the validation and uncertainties of the algorithm are described in detail in Part I. In this algorithm we use the three moments of the Doppler spectrum recorded by the MMCR: the radar reflectivity Ze, the Doppler velocity V_d, and the Doppler spectrum width σ_d. It can be shown (Gossard 1994) that a model describing these measurements can be derived by assuming a convolution between a population of cirrus particles and a turbulent spectrum with some mean vertical motion. Therefore, with an assumption of Rayleigh scattering (Evans and Stephens 1995) for cirrus particles at the 8-mm wavelength of the MMCRs, we further assume that the cirrus particle size distribution can be described as an exponential function (Heymsfield 2003) and that the atmospheric motions can be represented in terms of a mean vertical speed W_m and a double-sided exponential turbulent spectrum with an exponential slope of W_σ. With these assumptions, a forward model of the Doppler moments is inverted for the cirrus particle size distribution and W_m. The primary uncertainties of the algorithm are due to the basic assumptions of the algorithm and the need to represent the particle mass and area in terms of some representative particle habit. Using aircraft data, we determine in Part I that the uncertainties in ice water content (IWC) and mass-weighted diameter D_{mass} are 50% and 30%, respectively. In the analysis that follows, we apply the algorithm to many years of data and hundreds of thousands of cirrus volumes. We do not account for water vapor attenuation of the radar beam; however, this would bias the radar reflectivity by less than the uncertainty in radar measurements (Clothiaux et al. 1995).

We assume that the retrieval uncertainty is random so that errors of the mean values decrease as the inverse square root of the number of samples. Bias error in the retrievals is difficult to account for, however. Bias in the statistics would occur because of systematic differences between what we assume about the properties of the cirrus and what actually occurs on average. The potential sources of biases would be differences in the functional shape of the particle size distribution (i.e., bimodality) or the particle habit. Our sensitivity studies in Part I showed that the crystal habit assumption is, by far, the most significant source of potential bias. Although our comparison with in situ data in Part I suggests that the bias is minimal, those comparisons were conducted using ice crystal habits that were observed during the flights with which we compared, and the number of actual coincidences was too small to establish a high degree of confidence.

The ice crystal habits influence the retrieval results through the mass– and area–dimensional relationships as described in Part I. Throughout this work, we use mass– and area–dimensional relationships derived from measurements collected in cirrus above SGP during March of 2000 following the general approach of McFarquhar and Heymsfield (1997). If the actual ice crystal habits are systematically different during the periods under consideration here, then we would expect the statistics derived from the long-term data to be biased by some unknown amount. In Part I, we conducted a sensitivity study in which the mass– and area–dimensional relationships were varied by 20%, and we found that the IWC, D_{mass}, and W_m could vary as much as 75%, 17%, and 15 cm s^{-1}, respectively. We return to this topic below.

From the retrieved particle size distributions, cirrus properties such as the IWC, particle effective radius Re, mass-weighted maximum diameter D_{mass}, and mass-weighted fall velocity V_{fm} in the radar sample volumes are calculated as described in Part I. In addition, the optical depth is calculated using the area–dimensional relationships found in Mitchell et al. (1996). We note that because the weighted fall speed of a particle population depends on the ratio of distribution mass to cross-sectional area and the optical extinction depends primarily on the distribution cross-sectional area a retrieval of the distribution mass and fall speed implies a particle distribution cross-sectional area and thereby extinction and, when integrated over the layer, the optical depth.

The ice cloud processes that result in the derived microphysical properties are fundamentally related to updraft velocities within the cloud environment. A full understanding of cirrus cloud properties requires information of this dynamical environment. In this study, the dynamical properties are indicated by W_m in the radar resolution volumes. Given a 0.2° beamwidth, the hori-

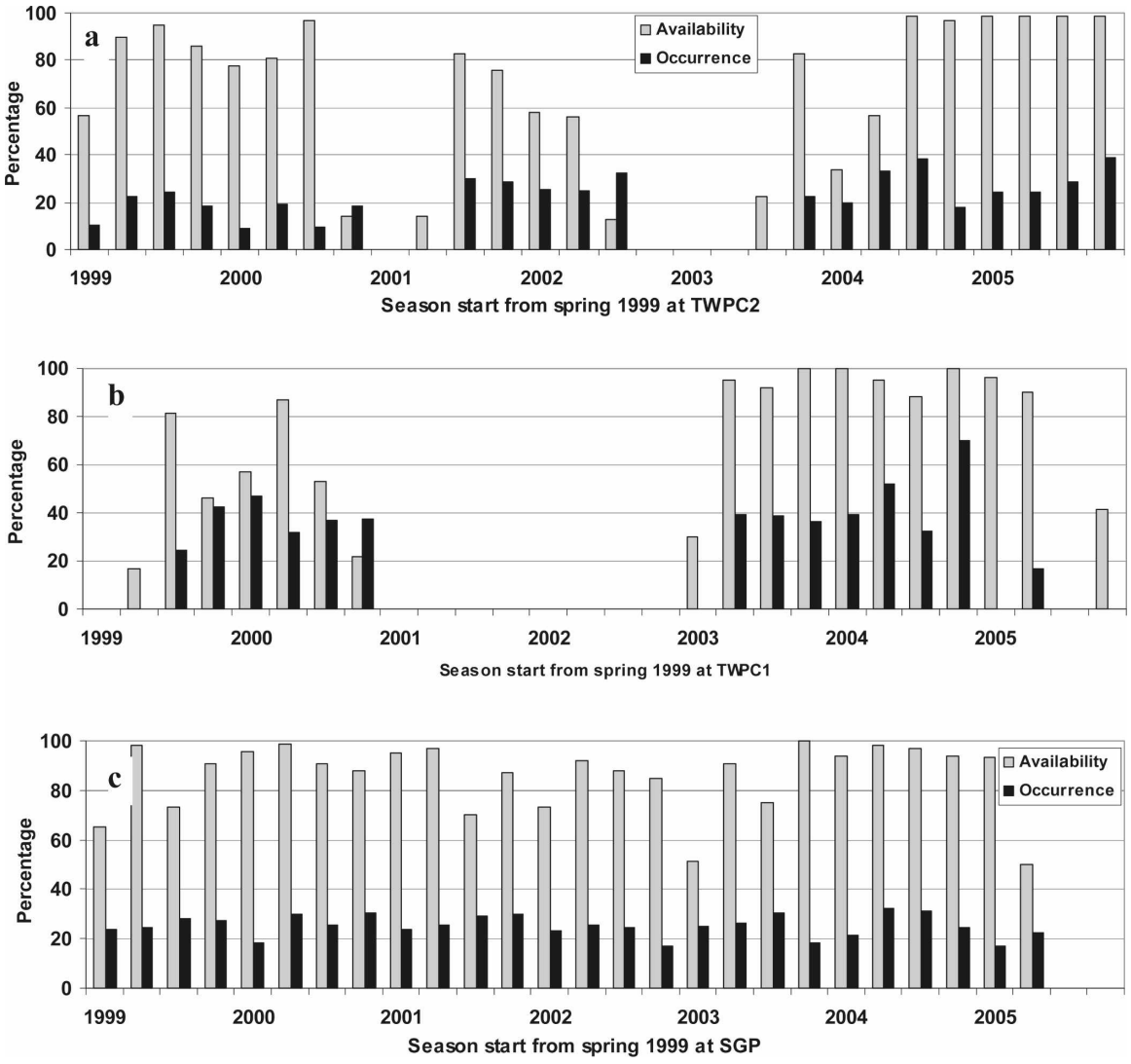

FIG. 1. The availability of MMCR observations (gray bars) and occurrence of cirrus (black bars) at the ARM (a) TWPC2, (b) TWPC1, and (c) SGP calculated for each season since spring 1999. At SGP, an operational mode important for cirrus analysis was inoperable after June 2005 although data from other operational modes are available.

zontal scale of measurements at cirrus altitudes is approximately 35 m with depths of 90 m. We assume that these scales approximate cloud-scale motions.

b. MMCR data availability

The MMCRs were designed to operate continuously and autonomously. However, there are significant time periods during which data were not collected because of instrument problems. The percentage of proper MMCR data collection is calculated for each season at the three sites and is shown in Fig. 1. The MMCR at SGP provided useful data more than 90% of the time. However, we do not use the MMCR observations from SGP after 2005 because of a failure of the operational mode that is most sensitive to thin cirrus—this mode outage continued through 2008. The MMCR at TWPC1 was inoperable for a 2-yr period from 2001, which seriously hampers our ability to evaluate seasonal trends at that site.

Among these MMCR observations, there are in total 11 379, 10 370, and 9873 h of cirrus observations at SGP, Manus, and Nauru, respectively. The cirrus cloud occurrence frequency is also plotted as a function of season in Fig. 1 for the three sites. The cloud occurrence frequency at SGP demonstrates a more obvious seasonal variation than in the tropics. This figure also indicates that the cirrus occurrence is greatest at

TWPC1 and least at TWPC2, as expected from their geographic placement relative to the western Pacific warm pool.

3. Analysis results

a. A general look at cloud properties at SGP and TWP

Histograms of cirrus cloud height, temperature, V_{fm}, D_{mass}, IWC, and the cloud-scale vertical velocity W_m observed at the three sites are shown in Fig. 2, along with radar reflectivity and Doppler velocity. The mean, median, mode, and standard deviation of these properties as well as other properties such as optical depth and cloud geometrical thickness are listed in Table 1 for all seasons. Given the different sensitivities of the MMCRs, the results at the SGP site are also calculated in terms of clouds with radar reflectivity larger than -40 dBZ, which is roughly the minimum signal at the TWP sites. The increased minimum reflectivity threshold at SGP excludes less than 10% of the total cirrus, which tend to be composed of smaller ice masses at relatively colder temperatures.

In general, the frequency distributions of IWC, particle size, and associated mass-weighted fall velocity in Fig. 2 are skewed. For example, the median and mode of the optical depth and ice water path (IWP) distributions are orders of magnitude smaller than the mean (Table 1). In the following seasonal and diurnal variability analyses, results are mainly shown in terms of mean rather than median or mode to avoid repetition, but the skewness of the distributions should be kept in mind. Figure 2 and Table 1 also show that, in general, the tropical cirrus clouds have slightly larger ice particles with greater mass, which correspond to larger V_{fm}.

The differences between the two TWP sites are not as large as the differences between the tropics and the midlatitudes. The temperature and height distributions illustrate that the cirrus clouds at Nauru are more peaked and have a relatively smaller variance than those above Manus, and the cirrus at both sites seem to have similar radar-observed top heights (note that the layer top observed by the radar is often negatively biased because of radar sensitivity, as found from analysis of lidar data in Comstock et al. 2002). The cirrus clouds at Manus have an enhanced probability distribution in the 8–10-km height range (see also Mace et al. 2006b). The enhanced probability of occurrence in the 8–10-km region at Manus may be attributed to a closer association with deep convection at that location and may also contribute to the enhanced probability of larger particle size, and IWP for cirrus observed at Manus.

For the cloud-scale vertical motions, the distribution of the vertical velocities at SGP is almost symmetrical between upward and downward motion with a $+2$ cm s^{-1} residual of the mean, while the cloud-scale vertical velocities in cirrus at the TWP sites suggest stronger mean upward motion with a residual of about $+10$ cm s^{-1}. There are also other reports of cirrus cloud–related vertical velocities observed at other scales using aircraft data. Gultepe and Starr (1995) investigated the cloud-scale dynamical structure and turbulence in cirrus using aircraft observations from the First International Satellite Cloud Climatology (ISCCP) Regional Experiment (FIRE). They found that a spectrum of phenomena exist with small-scale convective cells in the cloud system with associated updrafts of 40–70 cm s^{-1}, gravity waves (2–9-km wavelength), quasi-2D waves ($\sim$10–20-km scales) with up to 20 cm s^{-1} amplitude in vertical velocity, and mesoscale waves ($\sim$170-km wavelength) with associated vertical velocity amplitudes less than 3 cm s^{-1}. Intermediate-scale wave structures were also evident within cloud systems where the associated amplitude in vertical velocity was markedly greater, perhaps exceeding 50 cm s^{-1}. In Heymsfield (1977), using aircraft microphysical measurements and Doppler radar measurements, it was found that the vertical velocities typically range from 10 cm s^{-1} in warm-frontal overrunning systems to in excess of 50 cm s^{-1} in clouds associated with closed low or isolated convective cells. From wind profiler measurements over tropical islands, the mean vertical velocity in stratiform cloud regions above 9 km was observed to be in excess of 10 cm s^{-1} (Balsley et al. 1988; Gage et al. 1991, Jagannadha Rao et al. 2003). Mace et al. (2006a) found that midlatitude cirrus cloud structure and properties are found to be correlated with the large-scale vertical velocity on synoptic scales. On the cloud scale, cloud properties are related to the vertical distribution of ascending and descending air and its temporal change. As indicated in Heymsfield (1975), a cirrus uncinus cloud layer can be defined from top to bottom as generating, growing, and evaporating regions with updraft velocities of 1 m s^{-1} common in the generating regions.

The enhanced infrared absorption in high-altitude anvil and thin cirrus clouds results in positive heating rates as illustrated by Ackerman et al. (1988). Assuming that all heating is converted to vertical motions as in Ackerman et al. (1988), ascent rates for a radiatively active layer are given simply by $W = H/(d\theta/dz)$, where H is the heating rate. Assuming characteristic values of H (30 K day^{-1}) for thick cirrus, and $d\theta/dz = 3$ K km^{-1} (Garrett et al. 2005), we estimate $W \sim 10$ cm s^{-1}. However, the residual vertical motions found by averaging the retrieved vertical motions are about a factor of

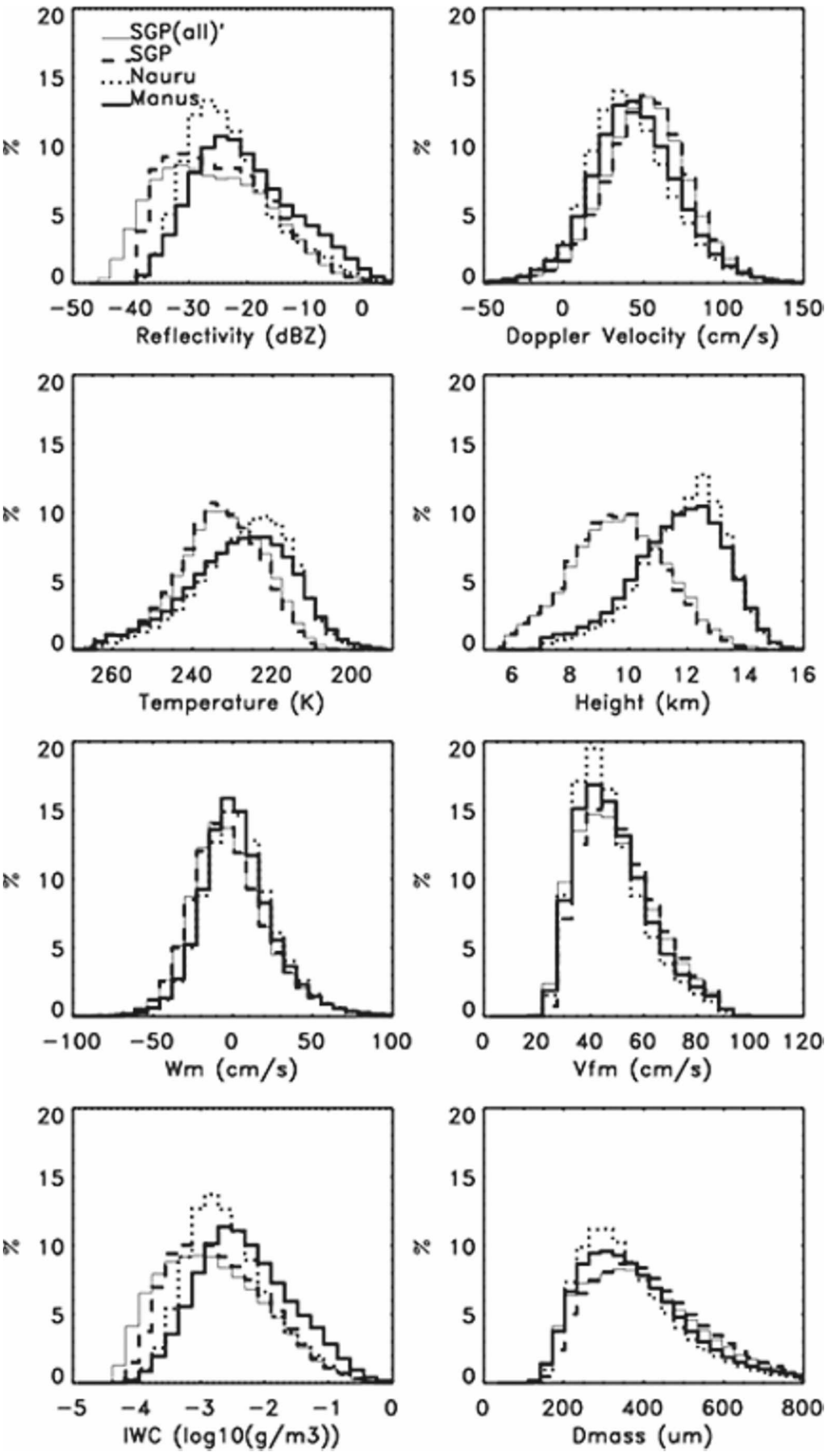

FIG. 2. Histogram of cloud properties such as cloud temperature, cloud height, in-cloud air vertical motion W_m, mass-weighted fall velocity V_{fm}, IWP (in logarithm base), and mass-weighted diameter D_{mass} for SGP (dashed line for 40-dBZ threshold and thin solid line for all), TWPC1 (Manus; solid line), and TWPC2 (Nauru; dotted line).

TABLE 1. Summary of mean and standard deviation of the retrieved cirrus cloud properties and air vertical motion at SGP, TWPC2, and TWCPC1 sites for all seasons and each season. The boreal spring, summer, autumn, and winter are denoted as MAM, JJA, SON, and DJF, respectively. The result for all seasons also includes median and mode in italics.

Sites	Season	Optical depth	IWP (g m^{-2})	Re (μm)	D_{mass} (μm)	V_{fm} (cm s^{-1})	Thickness (km)	Height (km)	Temperature (K)	W_m (cm s^{-1})
SGP (-40 dBZ)	All	2.4 ± 8.3	132.1 ± 111.7	47.0 ± 15.1	31.7 ± 156.1	55.6 ± 25.0	1.44 ± 1.02	9.0 ± 1.59	234.1 ± 10.7	4.8 ± 43.1
		0.2, 0.2	*5.0, 7.4*	*44.5, 41.6*	*281.5, 276.1*	*52.1, 50.0*	*1.01, 1.00*	*9.2, 9.3*	*233.9, 233.6*	*4.5, 4.7*
	MAM	2.0 ± 9.0	130.1 ± 101.6	48.1 ± 14.8	307.1 ± 90.3	51.7 ± 13.1	11.5 ± 1.00	9.3 ± 1.41	233.2 ± 9.5	5.7 ± 22.1
	JJA	3.0 ± 11.1	135.5 ± 151.1	50.1 ± 17.0	319.1 ± 171.7	56.9 ± 26.7	1.58 ± 1.20	9.7 ± 1.57	234.7 ± 11.6	6.9 ± 48.3
	SON	1.9 ± 9.6	131.1 ± 119.1	46.1 ± 17.1	297.1 ± 101.7	51.8 ± 14.8	1.21 ± 1.10	8.7 ± 1.51	235.1 ± 10.9	4.4 ± 12.9
	DJF	1.7 ± 2.6	76.01 ± 112.2	38.0 ± 17.7	295.1 ± 110.3	53.3 ± 18.4	1.38 ± 1.10	8.5 ± 1.28	232.5 ± 9.6	−4.9 ± 30.3
SGP	All	2.6 ± 9.0	133.1 ± 132.7	45.1 ± 20.4	296.4 ± 161.4	52.9 ± 25.4	1.54 ± 1.21	9.24 ± 1.64	233.2 ± 11.6	5.1 ± 31.0
		0.2, 0.4	*6.5, 8.0*	*42.3, 40.2*	*268.2, 257.1*	*51.9, 47.8*	*1.16, 1.15*	*9.32, 9.30*	*231.8, 231.9*	*5.4, 5.6*
	MAM	2.3 ± 9.4	137.8 ± 120.8	45.5 ± 15.9	290.1 ± 94.3	50.9 ± 14.3	1.25 ± 1.01	9.51 ± 1.41	231.1 ± 9.7	6.2 ± 24.4
	JJA	3.2 ± 10.8	165.5 ± 140.8	47.1 ± 26.4	299.7 ± 167.9	53.8 ± 26.3	1.61 ± 1.21	10.4 ± 1.64	233.6 ± 11.9	8.3 ± 35.8
	SON	2.2 ± 9.9	138.1 ± 129.4	43.1 ± 19.8	288.9 ± 103.5	50.1 ± 15.8	1.31 ± 1.12	8.9 ± 1.60	233.3 ± 11.1	5.4 ± 13.6
	DJF	2.0 ± 9.6	84.8 ± 29.4	41.6 ± 17.3	287.8 ± 110.7	51.8 ± 17.9	1.48 ± 1.01	8.8 ± 1.40	232.9 ± 9.4	−5.1 ± 29.4
TWPC2	All	1.90 ± 6.8	87.9 ± 95.9	47.4 ± 30.7	304.4 ± 186.0	50.7 ± 26.8	1.48 ± 1.06	11.4 ± 1.5	227.8 ± 11.6	14.8 ± 35.1
		0.3, 0.5	*10.6, 21.1*	*44.2, 42.7*	*298.2, 291.8*	*48.0, 62.1*	*1.13, 1.12*	*11.7, 11.5*	*225.9, 226.1*	*10.4, 10.1*
	MAM	1.9 ± 6.0	89.1 ± 76.2	53.8 ± 22.0	287.8 ± 170.1	48.1 ± 24.4	1.47 ± 1.0	11.1 ± 1.3	226.1 ± 10.3	13.1 ± 30.9
	JJA	2.1 ± 6.7	113.2 ± 93.1	59.3 ± 29.5	312.7 ± 183.2	51.1 ± 26.8	1.48 ± 1.2	11.1 ± 1.6	225.9 ± 12.4	14.8 ± 36.3
	SON	1.8 ± 6.1	76.1 ± 89.1	58.0 ± 24.3	301.1 ± 189.1	52.0 ± 21.0	1.45 ± 0.9	11.2 ± 1.4	231.1 ± 11.6	14.9 ± 41.8
	DJF	1.7 ± 5.1	84.0 ± 83.8	54.1 ± 24.8	297.3 ± 152.7	49.8 ± 22.5	1.5 ± 1.0	11.9 ± 1.7	225.1 ± 10.7	13.1 ± 31.2
TWPC1	All	4.6 ± 13.4	210.4 ± 111.4	50.6 ± 37.2	317.1 ± 112.2	53.1 ± 33.3	1.69 ± 1.37	11.2 ± 1.70	229.8 ± 14.2	12.6 ± 34.5
		0.8, 1.0	*29.8, 50.1*	*47.2, 47.5*	*301.6, 296.9*	*51.8, 63.1*	*1.32, 1.22*	*11.4, 11.2*	*228.5, 228.9*	*7.4, 7.0*
	MAM	4.4 ± 10.9	188.6 ± 114.1	47.1 ± 28.9	301.1 ± 111.9	52.8 ± 39.1	1.58 ± 1.40	11.6 ± 1.71	228.9 ± 14.4	9.8 ± 34.5
	JJA	4.9 ± 11.5	229.6 ± 150.3	49.6 ± 35.0	375.7 ± 115.1	56.5 ± 31.9	1.68 ± 1.40	11.2 ± 1.67	229.6 ± 13.7	13.3 ± 39.8
	SON	4.5 ± 12.1	209.4 ± 98.1	53.1 ± 29.9	325.1 ± 109.1	55.1 ± 28.2	1.59 ± 0.90	11.3 ± 1.68	229.2 ± 13.4	13.5 ± 36.1
	DJF	4.7 ± 9.4	199.1 ± 174.2	49.5 ± 35.8	303.8 ± 221.1	53.5 ± 31.7	1.69 ± 1.44	11.8 ± 1.74	231.6 ± 14.7	11.3 ± 30.1

1.5–2 greater than what is likely due solely to upper-tropospheric heating rates in cirrus. We cannot discount the possibility that the W_m residuals are biased because of a systematic particle habit difference between the tropical cirrus and the midlatitude cirrus from which we derived the mass– and area–dimensional relationships. However, observations collected during the Tropical Warm Pool International Cloud Experiment (May et al. 2008) showed that cirrus that are more than several hours removed from deep convection are composed primarily of bullet rosettes—the predominant ice crystal habit observed during the March 2000 intensive observing period from which the mass– and area–dimensional relationships were derived. Therefore, while a bias is possible, it is likely that a significantly positive residual in W_m in the tropical cirrus actually exists. According to the radiation modeling study in a recent paper (Corti et al. 2006), the lofting of air by cirrus heating provides a link between deep convection, the first stage of troposphere–stratosphere transport, and the third stage, the Brewer–Dobson circulation. Our results provide preliminary observational evidence of cloud heating–induced lofting in the tropics.

b. Interannual and seasonal variation of cirrus clouds in the midlatitudes and tropics

Cirrus properties vary as the dominant weather patterns shift because of seasonal or interannual changes in large-scale meteorological conditions. The seasonal variation of cirrus cloud properties has a direct bearing on climate sensitivity and must ultimately be simulated properly by numerical models if climate prediction is to be considered realistic (Sanderson et al. 2008). The interannual variations are illustrated well for our particular geographic locations (SGP and Nauru) in Fig. 3 with the monthly mean and standard deviation (vertical line) of cirrus macrophysical, microphysical, and dynamical properties starting from January of 1999. Figure 4 shows the composite annual variation of cloud properties at the SGP and Nauru sites. The mean and standard deviation of cirrus properties in the four seasons are also summarized in Table 1.

For midlatitude cirrus, there are significant seasonal variations (Fig. 3a) with more frequent, thicker clouds occurring during the summer than the winter. The seasonal variations of IWP, optical depth, and particle size basically follow a similar pattern with maxima and minima during the summer and winter, respectively. Similar seasonal variations of cirrus properties in the midlatitudes are reported in several papers. In Sassen and Campbell (2001), the cirrus macrophysical properties in terms of their seasonal and monthly means and variations are described from a 10-yr dataset collected from a University of Utah ground-based facility. Their study shows that midlatitude cirrus cloud-top heights typically correspond to the midlatitude tropopause during nonconvective periods. Using 6 yr of continuous vertically pointing cloud radar data collected at SGP, Mace et al. (2006a) found that the midlatitude cirrus in the warm seasons have relatively larger IWC and particle effective size than those in the cold seasons. However, the seasonal differences in IWC were not found by Wang and Sassen (2002), who used lidar–radar observations. This discrepancy is likely related to different instrumentation because the lidar signals can be attenuated during thick cirrus events while the radar penetrates optically dense cirrus layers and conversely the lidar is able to sense tenuous cirrus that the radar does not.

In Fig. 3b, the monthly-averaged cirrus cloud properties at Nauru seem to exhibit interannual variability with the mean cloud properties increasing on average from 1999 to 2003 and then decreasing thereafter. ENSO is the most important coupled ocean–atmospheric phenomenon that causes climate variability on interannual time scales in the equatorial western Pacific. Kent et al. (1995) and Fu et al. (1996) indicate that correlations exist between cirrus cloud cover and the Southern Oscillation index over the tropics. During a warm event with convection displaced eastward into the central equatorial Pacific, cloud cover decreases over the western Pacific, caused by generally subsident air over this region.

A multivariate ENSO index (MEI; Wolter and Timlin 1993) has been developed mainly for research purposes and is calculated using six main observed variables (sea level pressure, zonal and meridional component of surface wind, sea surface temperature, surface air temperature, and total cloudiness fraction of the sky). Negative values of the MEI represent the cold ENSO phase La Niña, and positive MEI values represent the warm ENSO phase El Niño. The MEI value from 1999 to 2005 is shown in Fig. 5b as cited from the National Oceanic and Atmospheric Administration (NOAA)/Earth System Research Laboratory Web site. The MEI tended to increase gradually from the moderate La Niña that peaked in late 1999. This gradual increase culminated in a weak El Niño event in early 2003. The MEI decreased but remained in the positive range thereafter.

To investigate further the large-scale dynamics near Nauru, we compute the monthly-averaged Hovmöller brightness temperature anomalies averaged between 10°S and 10°N latitude from 130°E to 180° longitude using Geostationary Meteorological Satellite and Geostationary Operational Environmental Satellite data. The result is shown in Fig. 5a. We find that the cold

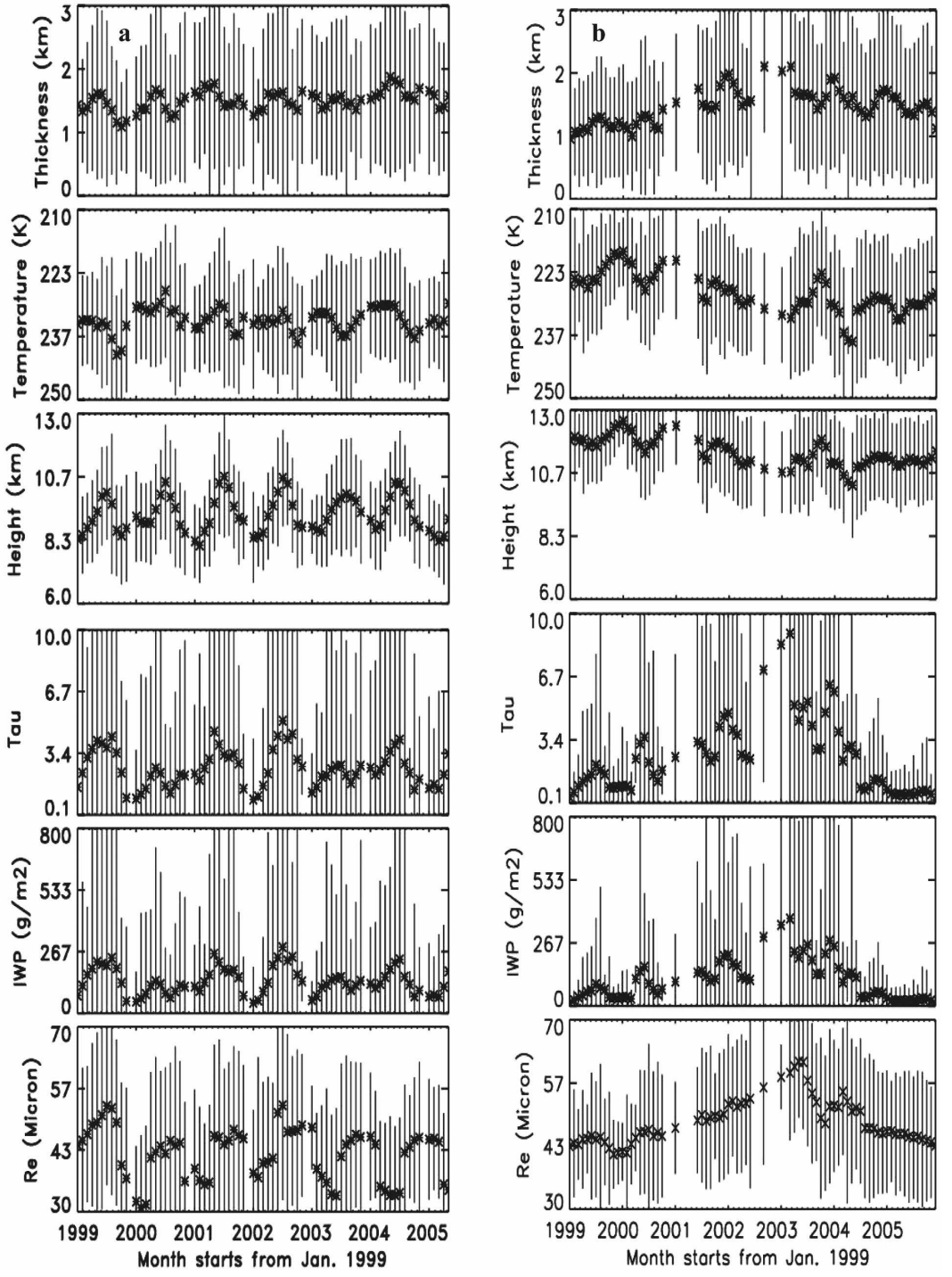

FIG. 3. Monthly variations of cirrus cloud properties observed at the ARM (a) SGP and (b) TWPC2 (Nauru) sites in terms of monthly mean (asterisks) and standard deviation (vertical bars).

anomaly generally moves eastward from 1999 and approaches Nauru in 2002 as the MEI increases, and it moves westward thereafter as the MEI decreases. The cloud monthly variations in Fig. 3b show that the cirrus thickness gradually increases, consistent with an increase in optical depth, effective particle size, and IWP. These values peak in mid-2002 through early 2003, following the peak of El Niño conditions. However, as the

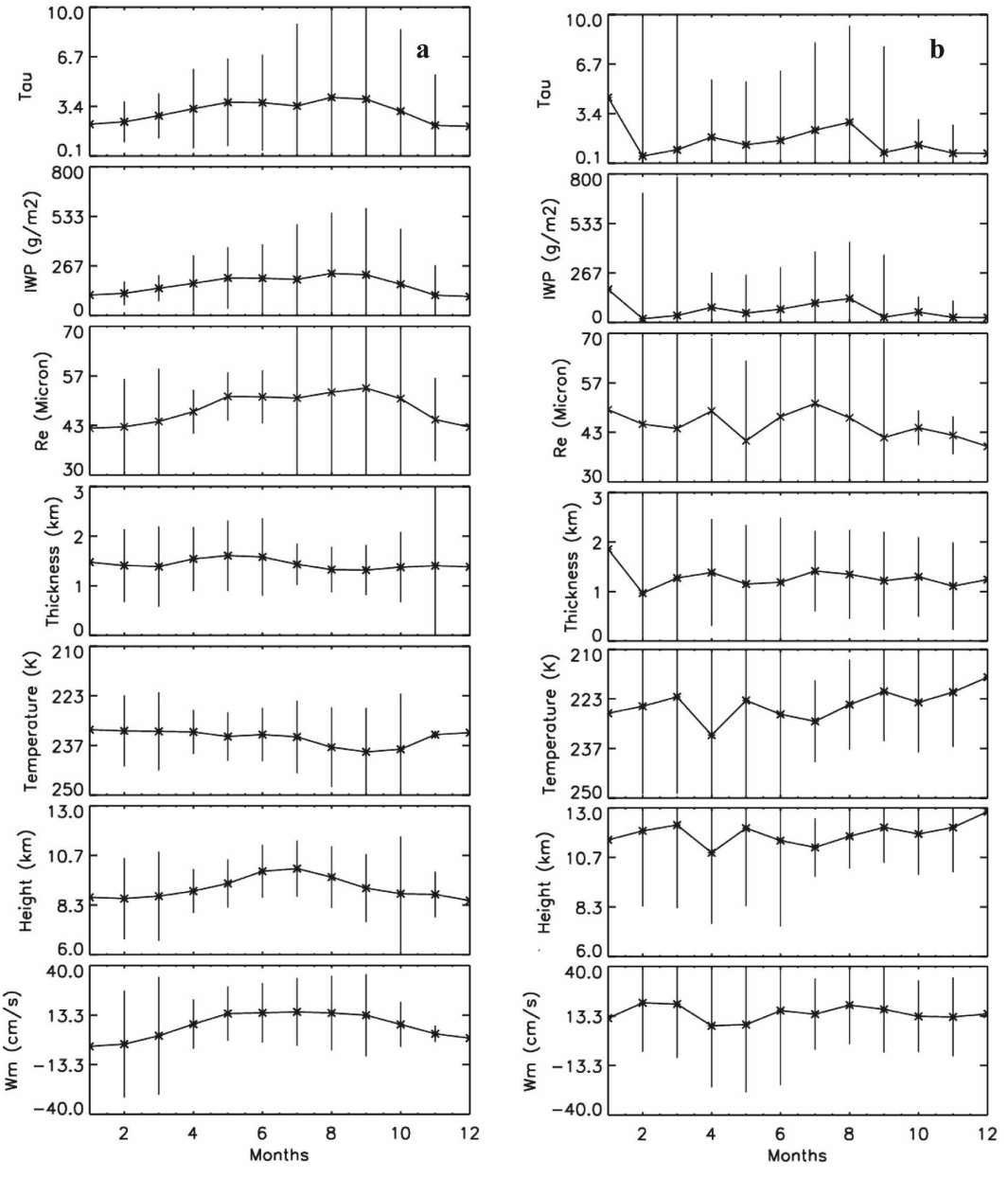

FIG. 4. The annual variations of cirrus cloud properties and in-cloud air vertical motion observed at the ARM (a) SGP and (b) TWPC2 (Nauru) in terms of composite monthly mean (asterisks) and standard deviation (vertical bars).

warm phase waned in later 2003, we find that the cloud properties' trends reverse, with decreasing optical depths, water paths, and smaller particle sizes. The correlation between monthly cloud property tendencies, such as Re and cloud-layer thickness, and the ENSO index is more than 0.7.

c. Diurnal variation of cirrus clouds in the tropics

The cloud properties and vertical motions are averaged by local hour to identify the diurnal cycles of various cloud properties. The hourly means and standard deviations are calculated from all samples in that hour from the 6-yr dataset to form a composite day.

The results at Manus and Nauru are shown in Fig. 6 as a function of local time. The macrophysical properties (cloud height, temperature, and cloud physical thickness) increase almost monotonically from midnight [0000 local time (LT)] to 1200 LT at both sites, followed by a decline thereafter. Only the cirrus observed at Manus show statistically significant variations

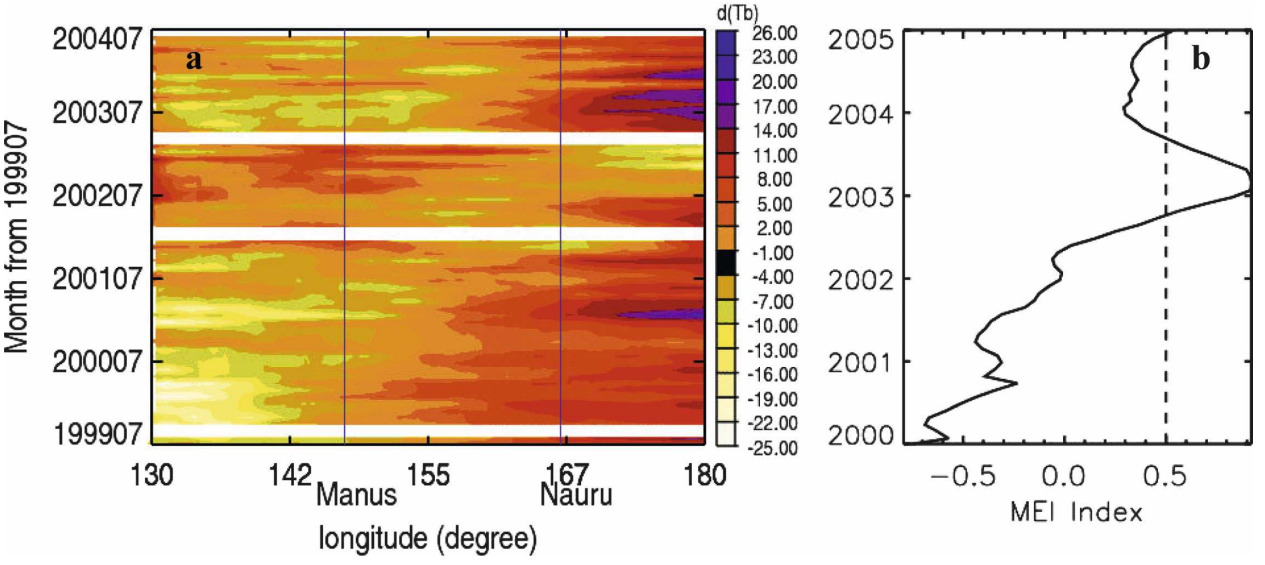

FIG. 5. (a) The Hovmöller diagram of monthly-averaged brightness temperature anomaly in the tropical 10°S–10°N latitude range from 130°E to 180° longitude. Negative values indicate cold anomaly caused by the increasing cold deep convective clouds, and positive values indicate warm anomaly. (b) The corresponding MEI.

in cloud microphysical properties, which increase in the morning from 0600 LT and peak in the early afternoon, then decrease thereafter. However the variations at Nauru are statistically insignificant because of the large standard deviation and subtle variations in the hourly averages.

The diurnal variation of in-cloud air motion at Manus shows a pattern that is similar to that at Nauru but with larger amplitude. The mean in-cloud vertical motion decreases from a maximum of +20 (Manus) and 15 (Nauru) cm s^{-1} around noon to an average of 5 (Manus) and 10 (Nauru) cm s^{-1} at local midnight.

d. Diurnal variation of midlatitude cirrus clouds in the summer and winter

A composite diurnal cycle of cirrus properties and in-cloud air motions of midlatitude cirrus compiled from all months is also analyzed as a function of local time, and there are no noticeable diurnal variations in the annual average. However, with such a significant transition in meteorological regime between winter and summer at SGP we do expect a strong sensitivity to season (Fig. 7). Although the diurnal cycle in W_m is small at SGP during both seasons, there is a seasonally dependent residual in W_m of approximately ± 5 cm s^{-1}. In the absence of significant heating during the winter when synoptic-scale motions are the primary dynamical forcing, we would expect a near-zero residual in W_m. The ± 5 cm s^{-1} residual found here might suggest a systematic bias attributable to the assumed microphysical habits.

Relative to the winter, the summer cirrus at SGP show obvious and significant diurnal variations in most cloud properties. The clouds are observed to be thicker and higher in the later afternoon (1600–2200 LT), whereas the in-cloud air motion has slightly stronger updrafts before that late-day peak in the thickness. The comparison between Figs. 7a and 7b further distinguishes the difference between the summer and winter seasons. During the winter when synoptic-scale weather systems are the predominant source of dynamical forcing, diurnal variations are totally absent. Summer cirrus tend to be higher in altitude and relatively thicker geometrically and optically. Most of all, the in-cloud air motion tends to be upward (5 cm s^{-1}) during the summer. For both the tropics and midlatitudes, the diurnal cycles of cloud height and thickness are in phase with each other whereas the vertical motion and particle size lead the thickness and condensed mass cycles by several hours. It seems plausible that ascent resulting from radiative heating is contributing to the formation and/or maintenance of the cirrus that generates larger particles followed by sedimentation and sublimation in the cirrus as the layers grow, although this speculation must be confirmed using cloud-process models and further analysis of the data.

4. Discussion and summary

Because cirrus clouds are a product of the regional weather processes that inject water vapor and condensate into the upper troposphere, it is expected that local

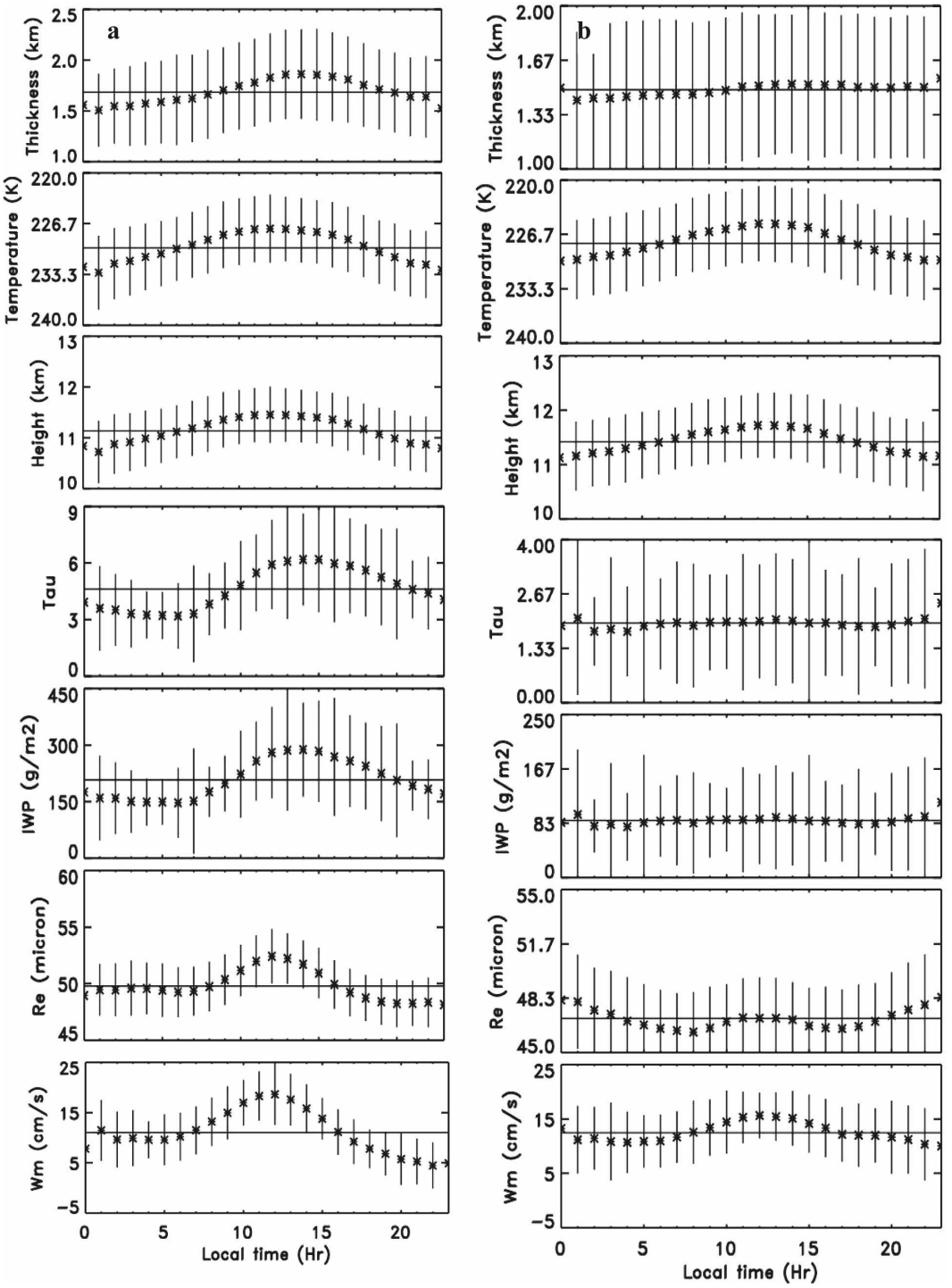

FIG. 6. The diurnal variations of macrophysical, microphysical, and dynamic properties of cirrus clouds at the ARM (a) TWPC1 (Manus) and (b) TWPC2 (Nauru) in terms of hourly mean (asterisks) and standard deviation (vertical bars). The horizontal line is the average of the hourly means.

cirrus cloud properties will depend significantly on geographic locations and regional meteorological behavior. The geographic dependence of cirrus properties is shown as a function of seasonal and diurnal time scales in the midlatitudes and tropics using measured and derived cloud properties. The generation mechanisms of cirrus at SGP mainly include synoptic disturbances as suggested in Sassen and Campbell (2001) during the

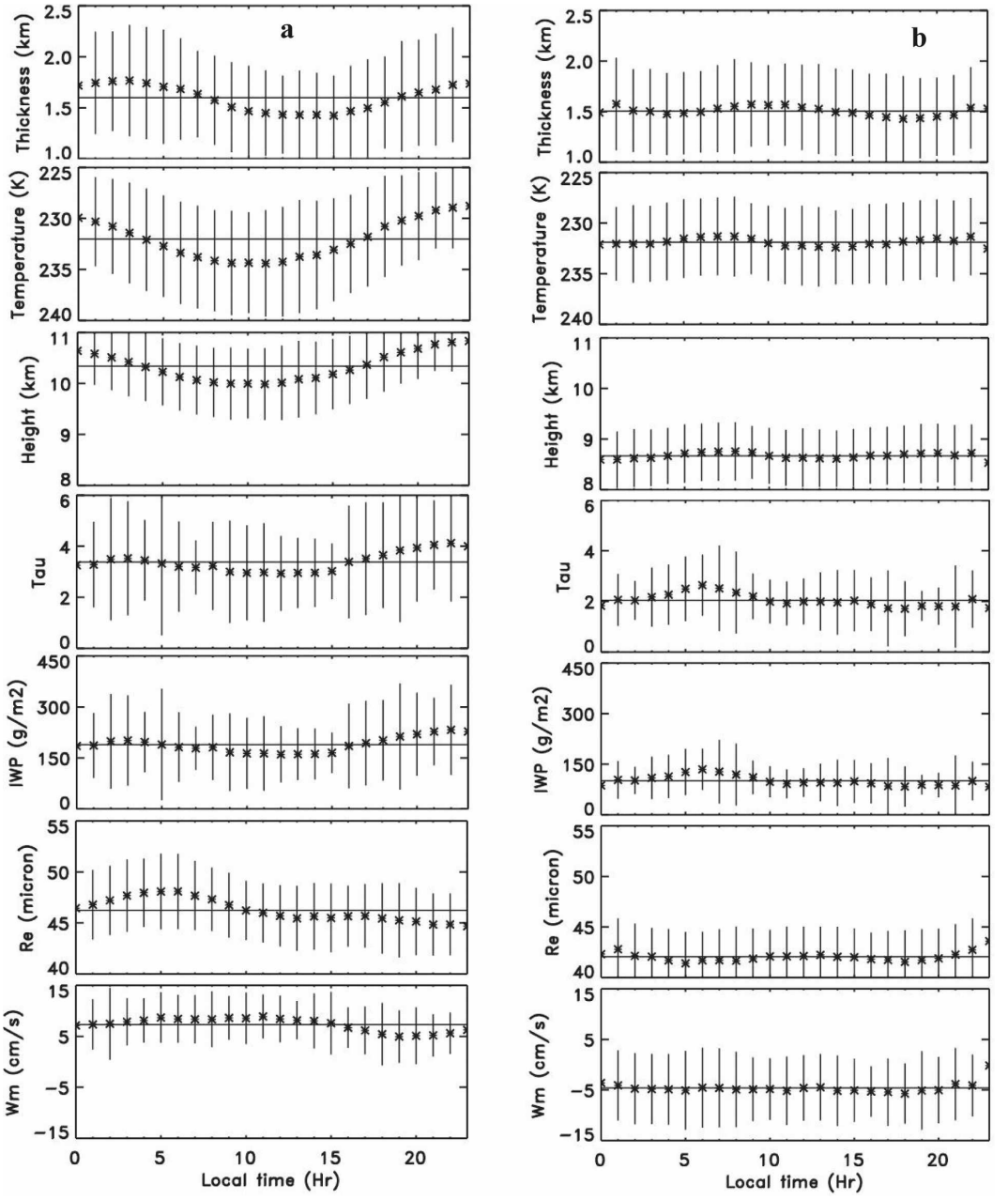

FIG. 7. The diurnal variations of cirrus cloud properties and in-cloud air vertical motion observed at the ARM SGP site during the (a) summer and (b) winter season in terms of hourly mean (asterisks) and standard deviation (vertical bars).

winter season although injection of condensate into the upper troposphere is more predominant during spring and summer. The cirrus clouds associated with synoptic-scale disturbances vary with season as the dominant weather patterns shift (Mace et al. 2006a). The seasonal dependence of cirrus frequency, cloud height, and temperature is clearly a reflection of the basic synoptic pattern. The increasing percentage of anvil cirrus cloud in the summer likely contributes to the increasing cloud optical depth and particle size.

For cirrus observed at the TWP Manus and Nauru Island sites, the main cirrus generation mechanisms are likely associated with deep convection that injects both condensate and water vapor into the upper troposphere (Mace et al. 2006b; Massie et al. 2002). Some combination of forcing mechanisms due to wave disturbances

and/or radiative heating away from convective sources is also likely. Because the condensate injected directly by deep convection quickly sediments and the mean particle sizes we find are large, in situ generation of cirrus must occur even though the large-scale atmosphere is generally gently subsident. Our findings show that interannual variations in cloud properties dominate the seasonal variation in the tropics. The observed cloud property variations are closely related to the proximity of deep convection, which is, in turn, sensitive to the tropical interannual variations such as ENSO. Sensitivity of cirrus properties to intraseasonal cycles such as the Madden–Julian oscillation is also expected, although the time series at the TWP sites are not sufficient to identify any correlations.

There are distinct differences in diurnal variations of cirrus observed at the SGP and TWP sites. Tropical cirrus clouds are observed higher in the atmosphere and are thicker in the morning and then decrease in the afternoon. The in-cloud air motion has a phase that is similar to that of the effective radius yet leads the other cloud properties by several hours. For cirrus clouds that occur during the winter at SGP, there is no obvious diurnal variation. However, the cirrus observed during the summer are also observed at higher altitude and in thicker layers during the afternoon following a weak midday maximum of in-cloud ascent. The diurnal cycle of tropical cirrus clouds and summer midlatitude cirrus seems to be in phase with the diurnal cycle of local deep convection with forcing because of radiative heating acting to maintain the layers following sedimentation of the initial injected condensate. For example, using the Tropical Rainfall Measuring Mission satellite measurements, Nesbitt and Zipser (2003) found that the number of mesoscale convective systems peaks during the predawn hours, probably because of the favorable nocturnal environment, whereas the mean coverage of convective systems peaks at noon as the stratiform part of the system expands. In a similar way, we find that the tropical cirrus, especially at Manus, increase in depth and water path on a nearly identical cycle.

Besides the differences in the seasonal/monthly and diurnal variations between the midlatitudes and tropics, the tropical ice clouds in general are very different from those found at the SGP site, with slightly larger particle sizes and ice masses, and they are more frequently associated with upward air motion. The positive residual of in-cloud air motion in the tropics may be observational evidence of the upwelling of air through cirrus radiative effects into the base of the TTL, which may, in turn, contribute to tropical troposphere–stratosphere transport. However, uncertainties in the predominant microphysical habits in the tropics and midlatitudes cause the actual magnitude of this phenomenon to be uncertain.

As demonstrated by this study, the ground-based long-term observations by the ARM Program provide the opportunity to study cirrus cloud properties in terms of monthly/seasonal and diurnal variations. In our continuing research, we will focus on the relationships among the cloud microphysical, macrophysical, and dynamical properties. For example, the cloud-scale vertical motion will be investigated as a function of height and temperature and as a function of calculated radiative heating. This study also highlights the need for a more exhaustive in situ database of cirrus microphysical properties. Remote sensing retrievals of cloud properties are inherently dependent on empirical knowledge of predominant ice crystal habits, and the current in situ dataset is insufficient for this purpose.

Acknowledgments. This research was supported by the Office of Biological and Environmental Research, Environmental Science Division, of the U.S. Department of Energy. Data were obtained from the Atmospheric Radiation Measurement Program. The MEI was obtained from the NOAA/Earth System Research Laboratory Physical Sciences Division Web site (http://www.cdc.noaa.gov/people/klaus.wolter/MEI/). We also thank three anonymous reviewers for comments and suggestions.

REFERENCES

Ackerman, T. P., and G. Stokes, 2003: The atmospheric radiation measurement program. *Phys. Today,* **56,** 38–45.

——, K. N. Liou, P. J. Valero, and L. Pfister, 1988: Heating rates in tropical anvils. *J. Atmos. Sci.,* **45,** 1940–1948.

Balsley, B. B., W. L. Ecklund, D. A. Carter, A. C. Riddle, and K. S. Gage, 1988: Average vertical motions in the tropical atmosphere observed by a radar wind profiler on Pohnpei (7°N latitude, 157°E longitude). *J. Atmos. Sci.,* **45,** 396–405.

Clothiaux, E. E., M. A. Miller, B. A. Albrecht, T. P. Ackerman, J. Velinde, D. M. Babb, R. M. Peters, and W. J. Syrett, 1995: An evaluation of a 94-GHz radar for remote sensing of cloud properties. *J. Atmos. Oceanic Technol.,* **12,** 201–229.

Comstock, J. M., T. P. Ackerman, and G. G. Mace, 2002: Ground-based lidar and radar remote sensing of tropical cirrus clouds at Nauru Island: Cloud statistic and radiative impacts. *J. Geophys. Res.,* **107,** 4714, doi:10.1029/2002JD002203.

Corti, T., B. P. Luo, Q. Fu, H. Vomel, and T. Peter, 2006: The impact of cirrus clouds on tropical troposphere-to-stratosphere transport. *Atmos. Chem. Phys.,* **6,** 2539–2547.

Del Genio, A. D., 2002: GCM simulations of cirrus for climate studies. *Cirrus,* D. K. Lynch et al., Eds., Oxford University Press, 310–326.

Deng, M., and G. Mace, 2006: Cirrus microphysical properties and air motion statistics using cloud radar Doppler moments. Part I: Algorithm description. *J. Appl. Meteor. Climatol.,* **45,** 1690–1709.

Duffy, P. B., G. Bala, P. J. Gleckler, K. E. Taylor, A. A. Mirin,

and M. E. Wickett, 2006: Global climate simulation in a multiscale modeling framework: Sensitivity to GCM-resolution. *Proc. Fall Meeting,* San Francisco, CA, Amer. Geophys. Union, A32B-04.

Evans, K. F., and G. L. Stephens, 1995: Microwave radiative transfer through clouds composed of realistically shaped ice crystals. Part I: Single scattering properties. *J. Atmos. Sci.,* **52,** 2041–2057.

Fu, R., W. T. Liu, and R. E. Dickson, 1996: Response of tropical clouds to the interannual variation of sea surface temperature. *J. Climate,* **9,** 616–634.

Gage, K. S., J. R. McAfee, D. A. Carter, W. L. Ecklund, A. C. Riddle, G. C. Reid, and B. B. Balsley, 1991: Long-term mean vertical motion over the tropical Pacific: Wind-profiling Doppler radar measurements. *Science,* **254,** 1771–1773.

Garrett, T. J., and Coauthors, 2005: Evolution of a Florida cirrus anvil. *J. Atmos. Sci.,* **62,** 2352–2372.

Gettleman, A, W. J. Randal, F. Wu, and S. T. Massie, 2002: Transport of water vapor in the tropical tropopause layer. *Geophys. Res. Lett.,* **29,** 1009, doi:10.1029/2001GL013818.

Gossard, E. E., 1994: Measurement of cloud droplet size spectra by Doppler radar. *J. Atmos. Oceanic Technol.,* **11,** 712–726.

Gultepe, I., and D. O. Starr, 1995: Dynamical structure and turbulence in cirrus clouds: Aircraft observations during the FIRE. *J. Atmos. Sci.,* **52,** 4159–4182.

Heymsfield, A. J., 1975: Cirrus uncinus generating cells and the evolution of cirriform clouds. Part II: Structure and circulations of the cirrus uncinus generating head. *J. Atmos. Sci.,* **32,** 809–819.

——, 1977: Precipitation development in stratiform ice clouds: A microphysical and dynamical study. *J. Atmos. Sci.,* **34,** 367–381.

——, 2003: Properties of tropical and midlatitude ice cloud particle ensembles. Part II: Applications for mesoscale and climate models. *J. Atmos. Sci.,* **60,** 2592–2611.

Jagannadha Rao, V. V. M., D. Narayana Rao, M. Venkat Ratnam, K. Mohan, and S. Vijaya Bhaskar Rao, 2003: Mean vertical velocities measured by Indian MST radar and comparison with indirectly computed values. *J. Appl. Meteor.,* **42,** 541–552.

Kent, G. S., E. R. Williams, P. H. Wang, M. P. McComick, and K. M. Skeens, 1995: Surface temperature related variations in tropical cirrus cloud as measured by SAGE II. *J. Climate,* **8,** 2577–2594.

Mace, G., G. Eugene, E. Clothiaux, and T. P. Ackerman, 2001: The composite characteristics of cirrus clouds: Bulk properties revealed by one year of continuous cloud radar data. *J. Climate,* **14,** 2185–2203.

——, S. Benson, and E. Vernon, 2006a: Cirrus clouds and the large-scale atmospheric state: Relationships revealed by six years of ground-based data. *J. Climate,* **19,** 3257–3278.

——, M. Deng, B. Soden, and E. Zisper, 2006b: On the association of tropical cirrus in the 10-15-km layer with deep convective source regions; An observational study combining millimeter radar data and satellite-derived trajectories. *J. Atmos. Sci.,* **63,** 480–503.

Massie, S., A. Gettelman, W. Randel, and D. Baumgardner, 2002: Distribution of tropical cirrus in relation to convection. *J. Geophys. Res.,* **107,** 4591, doi:10.1029/2001JD001293.

May, P. T., J. H. Mather, G. Vaughan, C. Jakob, G. M. McFarquhar, K. N. Bower, and G. G. Mace, 2008: The Tropical Warm Pool International Cloud Experiment. *Bull. Amer. Meteor. Soc.,* **98,** 629–645.

McFarquhar, G. M., and A. J. Heymsfield, 1997: Parameterization of tropical cirrus ice crystal size distributions and implications for radiative transfer: Results from CEPEX. *J. Atmos. Sci.,* **54,** 2187–2190.

Mitchell, D. L., S. K. Chai, Y. L. Liu, A. J. Heymsfield, and Y. Dong, 1996: Modeling cirrus clouds. Part I: Treatment of bimodal size spectra and case study analysis. *J. Atmos. Sci.,* **53,** 2952–2966.

Moran, K. P., B. E. Martner, M. J. Post, R. A. Kropfli, D. C. Welsh, and K. B. Widener, 1998: An unattended cloud profiling radar for use in climate research. *Bull. Amer. Meteor. Soc.,* **79,** 443–455.

Nesbitt, S. W., and E. J. Zipser, 2003: The diurnal cycle of rainfall and convective intensity according to three years of TRMM measurement. *J. Climate,* **16,** 1456–1475.

Sanderson, B. M., C. Piani, W. J. Ingram, D. A. Stone, and M. R. Allen, 2008: Towards constraining climate sensitivity by linear analysis of feedback patterns in thousands of perturbed-physics GCM simulations. *Climate Dyn.,* **30,** 175–190.

Sassen, K., 2002: Cirrus: A modern perspective. *Cirrus,* D. K. Lynch et al., Eds., Oxford University Press, 11–40.

——, and J. R. Campbell, 2001: A midlatitude cirrus cloud climatology from the Facility for Atmospheric Remote Sensing. Part I: Macrophysical and synoptic properties. *J. Atmos. Sci.,* **58,** 481–496.

Sherwood, S. C., and A. E. Dessler, 2003: Convective mixing near the tropical tropopause: Insights from seasonal variations. *J. Atmos. Sci.,* **60,** 2674–2685.

Stephens, G. L., S. C. Tsay, J. P. W. Stackhouse, and P. J. Flatau, 1990: The relevance of the microphysical and radiative properties of cirrus cloud on climate and climatic feedback. *J. Atmos. Sci.,* **47,** 1742–1753.

Wang, Z., and K. Sassen, 2002: Cirrus cloud microphysical property retrieval using lidar and radar measurements. Part II: Midlatitude cirrus microphysical and radiative properties. *J. Atmos. Sci.,* **59,** 2291–2302.

Wolter, K., and M. S. Timlin, 1993: Monitoring ENSO in COADS with a seasonally adjusted principal component index. *Proc. 17th Climate Diagnostics Workshop,* Norman, OK, NOAA/NMC/CAC, NSSL, Oklahoma Climate Survey, CIMMS, and the School of Meteorology, University of Oklahoma, 52–57.